

# Bond behavior in NSM-strengthened masonry

Hamid Maljaee<sup>1</sup>, Bahman Ghiassi<sup>2</sup>, Paulo B. Lourenço<sup>3</sup>

## ABSTRACT

Near Surface Mounted (NSM) reinforcement is an interesting technique for seismic strengthening of masonry and historical structures. Despite having several advantages compared to conventional techniques, little attention has been given to understanding the involved mechanisms (such as bond behavior) in the performance of masonry components strengthened with this reinforcement technique. This study presents an experimental and analytical investigation on the bond performance of NSM-strengthened masonry bricks aiming at filling the existing gaps in the available experimental results in the literature. The main focus is on the effect of test setup and bond length, but attention has also been given to the groove size and loading regime effect on the bond performance. The accuracy of the existing bond strength prediction models is also assessed and the required modifications are proposed.

*Keywords: Near Surface Mounted; Masonry; Strengthening; Bond; FRP; Experimental testing; Analytical modeling.*

---

<sup>1</sup>PhD Student, ISISE, University of Minho, Department of Civil Engineering, Azurém, 4800-058 Guimarães, Portugal. Phone: +351 253 510 499, fax: +351 253 510 217, E-mail: [h.maljaee.civil@gmail.com](mailto:h.maljaee.civil@gmail.com)

<sup>2</sup>Marie Curie IF Research Associate, Current address: Microlab, Department of Civil Engineering and Geosciences, TU Delft, Delft, The Netherlands. Phone: +31 15 2788741, E-mail: [bahmanghiassi@gmail.com](mailto:bahmanghiassi@gmail.com)

<sup>3</sup> Professor, ISISE, University of Minho, Department of Civil Engineering, Azurém, 4800-058 Guimarães, Portugal. Phone: +351 253 510 209, fax: +351 253 510 217, E-mail: [pbl@civil.uminho.pt](mailto:pbl@civil.uminho.pt)

# 1 Introduction

Fiber reinforced polymers (FRP) have been extensively used for strengthening of masonry and concrete structures due to advantages such as low weight, ease of application, corrosion resistance and high durability. These composites are generally used for Externally Bonded Reinforcement (EBR) or Near-Surface Mounted (NSM) strengthening techniques. The disadvantages related to the EBR strengthening techniques (such as special requirement for surface treatment and susceptibility to aggressive environmental conditions), promotes the use of NSM technique. Additionally, the NSM reinforcement does not change the aesthetics of the structure which is a great concern when dealing with restoration of historical structures [1,2]. NSM systems are also more efficient due to their larger bonded area to cross section ratio in comparison with EBR systems. The available literature on strengthening of masonry structures using NSM technique have shown its notable effect on increasing the ductility and capacity of the structures [3]. Despite these advantages, the available literature on characterization and performance assessment of NSM-strengthened masonry is still limited, see e.g. [3–6].

The NSM technique involves introducing FRP laminates or bars into slits prefabricated on the tensile face of structural elements using an epoxy adhesive [7]. In these systems, the stresses are transferred from the substrate to the reinforcing material through the adhesive and the interfacial stresses. The adhesive-to-substrate and the FRP-to-adhesive bond performance are therefore critical mechanisms. Although the bond performance has been subject of several studies in case of NSM-strengthened concrete elements, see e.g. [8–15], little attention has been given to strengthened masonry components, see e.g. [2,16–18]. The effect of different parameters (including the dimensions and shape, the adhesive type, the mechanical strength of substrate, the groove dimensions and the bonded length have been deeply investigated in NSM-strengthened

concrete components [1,2,8,19,20]. The available studies on NSM-strengthened masonry, has not yet fully covered all these parameters and is mostly devoted to the effect of bond length on limited types of substrate. The majority of available studies are devoted to large bonded lengths and the bond performance in short bonded lengths still remains unexplored.

This paper presents an experimental assessment of the bond performance in CFRP NSM-strengthened bricks with special attention to short bonded lengths to fulfill the current gap in the literature. Attention has also been given to the effect of test setup, groove dimensions and loading regime. Based on the produced experimental results and the available data in the literature, a survey is also performed on accuracy of the existing bond strength analytical models and suitable modifications are proposed.

## **2 Experimental program**

### **2.1 Specimens**

The specimens were composed of solid clay bricks with dimensions of 200 mm×100 mm×50 mm strengthened with S&P<sup>®</sup> CFRP strips made of unidirectional carbon fibers. The strips had 10 mm width and 1.4 mm nominal thickness. A two-part epoxy adhesive (S&P resin 220) was used to bond the CFRP strips to the bricks following the near surface mounted (NSM) strengthening technique.

For preparation of the specimens, rectangular grooves were initially cut on the bricks' surfaces by an electrical saw with the desired width and depth. Then the bricks were washed, cleaned and dried in an oven for 24 hours at 100°C. After cooling in the laboratory environment, the dust was removed from the grooves using an air compressor. The grooves were then filled with the epoxy up to half of its depth. The CFRP laminates were then carefully inserted into the grooves and were covered with another layer of epoxy. The position of the laminate inside the groove was controlled

by wrapping a tape around the laminate at both ends (outside of the bond area). The tapes also acted as a barrier to prevent penetration of the adhesive out of the bond zone, see Fig 1. The exterior surface of the tape was greased with oil to minimize the friction with the groove's perimeter during the tests.

The laminates were applied with different bond lengths (from 30 mm to 150 mm). A 40 mm unbonded length was left at the loaded end to avoid compressive crushing of the bricks during the tests due to the edge effects, see Fig 2. Two aluminum plates were glued at the end of the laminate to facilitate gripping of the specimens during the tests. The specimens were cured in laboratory conditions for two weeks as suggested in the technical datasheets provided by the manufacturer. The specimens are labeled according to the groove width (G) and bond length (B), throughout the paper.

## 2.2 Material properties

The compressive strength of the bricks was experimentally obtained as 16.7 MPa. The tests were performed on 40 mm×40 mm×40 mm cubes following the instructions given in ASTM C67 [21] and EN 772-1 [22]. The tests were conducted under force-controlled conditions at the rate of 150 N/min. To reduce friction, a pair of free-friction Teflon papers (with oil in the middle) was placed between the specimens and the compression plate. Application of the correction factor proposed in ASTM C39/C39M [23] to consider the specific dimensions of the specimens (factor of 0.87 for a height-to-length ratio of 1) lead to a compressive strength of 14.5 MPa as presented in Table 1.

The epoxy adhesive had a 14 days tensile strength and elastic modulus of 22 MPa and 7.15 GPa, and the CFRP laminate had an elastic modulus of 165 GPa, respectively according to [24]. The summary of the materials' mechanical properties is presented in Table 1.

### 2.3 Test setup

As no standard test method is available for investigating the bond behavior in NSM-strengthened concrete or masonry specimens, various test setups have been employed by different researchers.

A single-lap shear test scheme, by fixing the specimens to a supporting frame from the bottom and pulling the laminate from the top, is often used for this purpose. The specimens are fixed using a rigid restraining plate placed on top of the specimens which, after initial adjustments, is anchored to the supporting frame from the bottom. This leads to application of a pre-compression load to the specimens before starting the tests which can influence the experimental results [5]. Regardless of the advantages and disadvantages of this test setup, the specific geometry and size of the specimens did not allow to use such a system for performing the tests in this study.

The single-lap shear bond test setup developed in [25,26] for characterization of the bond behavior in EBR-strengthened bricks was thus used here, see Fig 2. This test setup was not directly applicable for NSM-strengthened specimens due to the geometrical differences of the specimens compared to the EBR-strengthened specimens. In EBR strengthening technique, the FRP sheet is applied on the substrate's surface, while in NSM technique the laminate is inserted inside the specimen for few millimeters. The clamping and restraining systems were thus changed in two stages to optimize the test setup, see Fig 3. In the original test setup, called Class 1 hereafter, the L-shaped plate used for supporting the specimens from top allowed partial restraining of the specimens. Lateral clamping, consisting of four individual clamps, were also used to avoid rotation of the specimens during the tests. In the second test setup, called Class 2 hereafter, the top supporting plate was modified to allow a full restrain. The clamping system consisted of four individual clamps and a free end restraining plate according to the details shown in Fig 3. Finally, in the third test setup, called Class 3, the full top restraining system (used in Class 2) with an edge

restrain-clamping system were used. The results obtained in each test setup are presented and compared in section 3.2. Based on the obtained results, the best test setup was chosen to investigate the effect of different parameters on the bond performance in NSM-strengthened bricks.

For performing the tests, the specimens were positioned on a rigid steel frame and restrained carefully from top and firmly clamped to the frame according to the details discussed in the last paragraph, see Fig 2. A servo-hydraulic system with a maximum capacity of 25 kN was used for performing the tests. The tests were driven under displacement controlled conditions with reference to the internal LVDT of the system by pulling the laminates with a velocity of 0.3 mm/min. The resultant load was measured by the load cell integrated in the testing machine. One LVDT was also placed at the loaded end to measure the relative slip between the laminate and the substrate, see Fig 2.

#### 2.4 Test parameters

The test parameters included the bond length, the groove size and the loading conditions (static and cyclic). To investigate the effect of the groove size, two different sizes in combination with different bond lengths of 30, 60 and 90 mm were considered. The groove sizes were 13 mm (depth)×3 mm (width) and 15 mm (depth)×5 mm (width). Three specimens were prepared for each groove size and bond length in this stage resulting in a total of 18 specimens. After analysis of the results, the larger groove size, which also showed a better bond performance, was selected for preparation of the next set of specimens.

Another group of specimens were prepared for investigating the effect of bond length. These specimens were prepared with the groove dimensions of 15 mm(depth)×5 mm and bond lengths of 30, 60, 90, 120 and 150 mm. Five specimens were prepared for each bond length resulting in a total of 25 specimens in this stage.

Both of the above mentioned groups of specimens were tested under monotonic displacement-controlled conditions with the rate of 0.3 mm/min. Three additional specimens with 15 mm (depth)×5 mm groove size and 150 mm bond length were also prepared for performing the tests under static cyclic loading regime. These tests were conducted with a constant displacement rate of 0.6 mm/min. The tests were performed under incremental cyclic displacements (with the internal LVDT as reference), with three consecutive cycles at each displacement level. The tests were continued until occurrence of delamination. The load history and the summary of loading conditions are presented in Fig 4 and Table 2.

### **3 Experimental results**

#### **3.1 Typical failure modes**

Three distinct failure modes were generally identified in the tested specimens as presented in Fig 5: (A) flexural splitting of the bricks at the free end; (B) debonding of the laminate from the brick substrate (at the adhesive-to-brick interface) accompanied by diagonal cracks inside the brick and (C) failure at the adhesive-to-brick interface. The effect of different parameters and test conditions on the failure mode of the specimens are discussed in the following sections. The observed failure mode (A) seems not to be realistic and thus, this type of failure is attempted to be avoided through changing the test parameters.

#### **3.2 Effect of test setup**

The typical force-slip curves and failure modes obtained from each test setup are presented in Fig 6. A clear change of failure mode and increase in the bond strength can be observed in the third test setups in comparison to the first one. Most of the partially restrained specimens (class 1 test setup) showed a combination of failure modes A and B. This seems to be due to the eccentricity of the load and the induced flexural stresses on the specimens. Fully restraining of the specimens

in test setup class 2 led to significant increment of the debonding load with the dominant failure modes of B and C. From the experimental results, it was concluded that the occurrence of failure mode B was partly due to the clamping system in these specimens. A different clamping system (full edge restraining) was therefore used in the test setup class 3. This change led to occurrence of adhesive-to-brick interface delamination (with the exception of only two specimens that had failure modes A and B) in the specimens tested in class 3 test setup. Again, significant increment was observed in the delamination force or force-slip curves in the specimens tested in test setup class 3 in comparison with those tested in test setup class 2. This test setup (class 3) was therefore chosen for performing the next tests.

### 3.3 Groove size

The effect of groove size on the bond behavior has been the subject of several studies in case of NSM-strengthened concrete components [8,13,27,28]. In general, it is believed that increment of groove dimensions can lead to decrement of stresses inside the substrate (as the stress transfer area increases). This can lead to increment of failure load if the failure mode remains unchanged (i.e. inside the substrate). In other cases, where the failure mode has changed to adhesive failure, the failure load has shown insignificant changes. These results show that the groove size can be optimized, based on the mechanical properties of the substrate and adhesive, to obtain the maximum bond strength in the reinforced system.

In case of NSM-strengthened masonry, the available results on the effect of groove size are still very limited but the mechanisms are expected to be similar to NSM-concrete systems. Among the few available studies, Dizhur et al. [5] investigated the effect of groove dimensions on the bond behavior in NSM-strengthened masonry prisms. They observed that increasing the groove width from 3 mm to 12 mm had no influence on the ultimate debonding load as all the specimens failed



by adhesive interfacial debonding. Increasing the depth of the groove, however, led to the change of failure mode to splitting of the brick, but the debonding load remained unchanged.

The tests performed in the current study showed a significant influence of the groove size on the debonding load. The variation of the debonding load,  $f_{ut}$ , with groove size is presented in Fig 7 for specimens with different bonded lengths. It can be observed that increasing the groove dimensions led to 51%, 45% and 44.5% increase in debonding force in the specimens with 30, 60 and 90 mm bond length, respectively. The effect of groove dimensions is similar in all bonded length. As both the groove depth and width were changed simultaneously, the effect of each parameter cannot be investigated separately. The failure mode (B) was the dominant failure mode in specimens with smaller groove dimensions (G1), while, failure mode (C) was mostly observed in the specimens with larger groove dimensions (G2).

### 3.4 Bond length

The effect of bond length has been extensively investigated in case of NSM-strengthened concrete components [8,13,27,28]. In case of NSM-to-masonry, the available results are again limited, see e.g. [29,30], and mostly devoted to bonded lengths in the range of 180 mm to 560 mm [5,18,30]). A clear understanding of the bond performance in short bonded lengths is missing but critical for masonry components. This is due to the short distance between the mortar joints (usually around 100 mm) where there is the highest possibility of cracking. The current study is therefore focused on characterization of the bond performance in short bonded lengths (ranging from 30 to 150 mm). The influence of bonded length on the force-slip response (envelopes) and the debonding force are presented in Fig 8. The coefficient of variation (CoV) of the results was in the acceptable range of 5 to 10%. The force-slip curves show that the debonding force,  $f_{ut}$ , and its corresponding slip, increase with increment of the bonded length as also reported in the literature, see e.g. [1,5]. On

the other hand, it seems that the initial stiffness of the force-slip curves slightly decreases with increment of the bonded length. The changes of the debonding force seem to become insignificant in the specimens with bond lengths longer than 120 mm. This observation shows that the effective bond length,  $l_e$ , is in the range of 120 mm to 150 mm in these specimens. Increment of the bond length also influenced the failure mode in each test setup class. Improvement of the failure mode from mode A to mode B was observed in class 1 set setup with increasing the bond length from 30 mm to 90 mm. In the same range of bond length, failure mode C dominantly occurred in the specimens tested in class 2 setup. In test setup class 3, besides two specimens that failure modes A and B in 30 mm and 60 mm bonded length range, most of the specimens had failure mode C in all bonded lengths. One can track the changes of failure modes in each class of test setup due to variation of bond length in Fig 9.

### 3.5 Cyclic loading

The force-slip response of the specimens tested under quasi-static cyclic loading is illustrated in Fig 10a. The results are presented in comparison with the static tests results. It can be observed that the cyclic loading considered in this study shows insignificant effect on the ultimate debonding load. Although it should be noted that the number of considered cycles in this study are limited and a different behavior maybe observed when larger number of cycles are considered. Different observed behaviors in the specimens may be due to material variability and the different applied load history, see Fig 10a. Therefore, further experiments are required to confirm the effect of cyclic loading on the FRP-brick bond behavior. An in-cycle reduction of strength can, however, be observed in each deformation range. This reduction is more obvious in higher load levels. The in-cycle degradation trend in each cyclic set is illustrated in Fig 10b. A similar trend was also reported in [17,18].

## 4 Existing bond strength predictive models

Numerous models can be found in the literature for predicting the bond strength in NSM-strengthened concrete components [1,10,12,31,32]. Whereas, due to the lack of enough experimental data, few models exist for NSM-strengthened masonry elements [5,18,30]. These models, although not always clearly separable, can be generally categorized as (a) empirical models proposed based on regression analysis of experimental data or (b) fracture mechanics based models. Among the available models in the literature, three existing models recently proposed for NSM-masonry elements [18,30] and two existing models proposed for NSM-concrete [10,31] are reviewed in this section. The accuracy of these models in predicting the bond strength in NSM-strengthened masonry is then evaluated in Sec. 5.

### 4.1 Model proposed by Seracino et al. [10]

Seracino et al. [10] proposed a generic model for EBR and NSM-strengthened concrete elements. The model was developed based on equilibrium and compatibility equations of laminate-to-concrete joints with the assumption of a predefined failure plane inside the concrete (cohesive failure mode in the substrate) and a triangular bond-slip law. The model was validated and its parameters were optimized by nonlinear regression analysis of a set of experimental data. Assuming that the local bond-slip law parameters (i.e. maximum shear stress and maximum slip), and the shape of the failure plane have direct influence on the bond strength in NSM-concrete joints, the debonding load,  $P_{\max}$ , was defined as:

$$P_{\max} = \sqrt{\tau_{\max} s_{\max}} \sqrt{L_{\text{per}} (EA)_p} \quad (1)$$

where,  $\tau_{\max}$  is the shear bond strength in the bond-slip law,  $s_{\max}$  is the slip corresponding to the  $\tau_{\max}$ ,  $L_{\text{per}}$  is the length of the debonding failure plane,  $E$  is the laminate's elastic modulus and  $A$  is the cross section area of the laminate.  $\tau_{\max} \times s_{\max}$  and  $L_{\text{per}}$  are defined as:

$$1 \quad \tau_{\max} s_{\max} = 0.976 \varphi_f^{0.526} f_c^{0.6} \quad (2)$$

$$2 \quad \varphi_f = \frac{d_f}{b_f} \quad (3)$$

$$3 \quad L_{per} = d_f + 2b_f \quad (4)$$

4 where,  $f_c$  is the cylindrical compressive strength of concrete, and  $d_f$  and  $b_f$  are the length of the  
5 failure plane perpendicular and parallel to the substrate surface, respectively. Substituting Eqs. (2-  
6 4) into Eq. (1), gives:

$$7 \quad P_{\max} = 0.988 \varphi_f^{0.263} f_c^{0.3} \sqrt{L_{per} (EA)_p} \quad (5)$$

8 The effective bond length (the length beyond which the maximum debonding resistance can be  
9 obtained),  $L_e$ , can be calculated as:

$$10 \quad L_e = \frac{\pi}{2\lambda} \quad (6)$$

$$11 \quad \lambda^2 = \frac{\tau_{\max} L_{per}}{s_{\max} (EA)_p} \quad (7)$$

12 where, the  $\tau_{\max}$  and  $s_{\max}$  are obtained based on a statistical analysis as:

$$13 \quad \tau_{\max} = (0.802 + 0.078 \varphi_f) f_c^{0.6} \quad (8)$$

$$14 \quad s_{\max} = \frac{0.976 \varphi_f^{0.526}}{0.802 + 0.078 \varphi_f} \quad (9)$$

15 It can be observed that  $\tau_{\max}$  is a function of compressive strength and  $\varphi_f$ , while  $s_{\max}$  is only a  
16 function of  $\varphi_f$  in this model. For obtaining the debonding resistance for bonded lengths less than  
17 the effective bond length ( $L < L_e$ ), application of a reduction factor ( $= L < L_e$ ) according to Eq. (5) is  
18 proposed [10].

#### 4.2 Model proposed by Zhang et al. [31]

Zhang et al. [31] used fracture mechanics approach for proposing an analytical formula for bond strength in NSM-concrete systems. In this model the debonding load is obtained as follows:

$$P_{\max} = \beta_L \sqrt{2G_f (EA)_p C_{\text{failure}}} \quad (10)$$

where  $G_f$  is the interfacial fracture energy,  $\beta_L$  is a parameter taking into account the effect of bond length, and  $C_{\text{failure}}$  is the perimeter of the failure surface which is obtained as the sum of the three side lengths of the groove. Interfacial fracture energy can be obtained as [33]:

$$G_f = 0.4\varphi_f^{0.422} f_c^{0.619} \quad (11)$$

where,  $\varphi_f$  can be obtained from Eq. (3). For the proposed model, the effective bond length is expressed as:

$$L_e = \frac{1.66}{\eta} \quad (12)$$

where

$$\eta^2 = \frac{\tau_{\max} C_{\text{failure}}}{2G_f (EA)_p} \quad (13)$$

and  $\tau_{\max}$  was obtained through regression analysis of numerical results, as:

$$\tau_{\max} = 1.15\varphi_f^{0.138} f_c^{0.613} \quad (14)$$

The parameter  $\beta_L$  is equal to 1 if  $L_b \geq L_e$ , and can be obtained as follows when  $L_b < L_e$  (was obtained as the best fit of experimental results):

$$\beta_L = \frac{L_b}{L_e} (2.08 - 1.08 \frac{L_b}{L_e}) \quad (15)$$

#### 4.3 Model proposed by Willis et al. [31]

Willis et al. [30] modified the model proposed by Seracino et al. [10] for application to NSM-masonry systems. They proposed to use the masonry flexural tensile strength,  $f_{ut}$ , instead of

cylindrical compressive strength in Eq. (5). Substituting the flexural tensile strength, obtained from Eq. (16), into Eq. (5) gives the bond strength as presented in Eq. (17).

$$\sqrt{f_c} = \frac{f_{ut}}{0.53} \quad (16)$$

$$P_{\max} = 1.45\phi_f^{0.263} f_{ut}^{0.6} \sqrt{L_{per}(EA)_p} \quad (17)$$

In this model, the authors propose to use the same equations as Eqs. (6-9), for obtaining the effective bond length in NSM-strengthened masonry.

#### 4.4 Model proposed by Kashyap et al. [18]

Kashyap et al. [18] proposed two formulas for strengthened masonry components: (1) a generic formula for both EBR and NSM strengthening systems, Eq. (18), and (2) a specific formula for NSM-strengthening systems, Eq. (19):

$$P_{\max} = 1.99\phi_f^{0.19} f_{ut}^{0.47} \sqrt{L_{per}(EA)_p} \quad (18)$$

$$P_{\max} = 2.63\phi_f^{-0.12} f_{ut}^{0.47} \sqrt{L_{per}(EA)_p} \quad (19)$$

It can be observed that the flexural strength of the masonry is used in both equations for obtaining the bond strength. Moreover, both equations have a similar form with the only difference in the values of the parameters (fitted with experimental data). In this model, Eq. (6) is proposed for obtaining the effective bond length but by using the following formulas for  $\tau_{\max}$  and  $s_{\max}$  :

$$\tau_{\max} = 8.83\phi_f^{0.15} f_{ut}^{0.2} \quad (20)$$

$$s_{\max} = 0.45\phi_f^{0.23} f_{ut}^{0.74} \quad (21)$$

In contrary to Eqs. (8-9), it can be observed that Kashyap et al. [18] considered that both  $\tau_{\max}$  and  $s_{\max}$  are dependent on the tensile strength of masonry unit and the aspect ratio of the failure plane ( $\phi_f$ ).

## 5 Assessment of accuracy of existing models

The accuracy of the existing models (presented in the last section) in predicting the maximum debonding force in NSM-strengthened masonry components is evaluated in this section. A database of experimental results on NSM-strengthened masonry components is initially formed. The database consisted of 70 experimental results available in the literature [2,5,16–18,30] and the experimental results produced in the current study, leading to a total of 103 test records. As the existing bond strength models are based on the assumption that failure occurs inside the substrate (cohesive failure), the specimens with sliding or adhesive failure were removed from the database. The final database, therefore, consisted of 89 bond test results in total as presented in Table 3.

A comparison is made between the bond strength predictions and the experimental results. The results are presented in Table 4 and Fig 11. The first two models, i.e. Seracino et al. [10] and Zhang et al [31], proposed for concrete elements showed a very low  $R^2$  values with respect to the experimental results and thus completely failed to predict the bond strength in NSM-strengthened masonry components, see Fig 11. On the other hand, the models proposed by Willis et al [30] and Kashyap et al [18] produced better predictions. It seems that the model proposed by Kashyap et al. (NSM) shows the best correlation with the experimental database, with an  $R^2$  of 0.85. Contrarily, the predictions are not reasonable for specimens with short bond lengths ( $l < 150$  mm), having an  $R^2$  ranged between 0.52-0.64. The model proposed by Willis et al. [30], however, failed to predict the debonding force of specimens with short bond length. This can be due to the overestimation of the effective bond length and the proposed reduction factor in this model. The effective bond length of the specimens tested in the current study was estimated to be in the range of 120 to 150 mm. However, the model proposed by Willis et al. [30] predicts the effective bond length of around 260 mm~290 mm, see specimen ID 57-89 in Table 4. This larger effective bond

length in comparison to the experimental results, leads to application of a larger reduction factor and thus underestimation of the bond strength.

## 6 Proposed model

Most available bond strength models for NSM-strengthened masonry systems [18,30], are developed based on modification of the model proposed by Seracino et al. [10]. The flexural tensile strength of the masonry is generally substituted for the cylindrical compressive strength and the other parameters are modified based on the best fit with the available experimental data. Although the predictions were in an acceptable range in the model proposed by Kashyap et al (NSM) [18], Fig 11d, it seems that some improvements can still be done for predicting the bond strength of specimens with short bond lengths. Additionally, the predictions of the effective bond length were not accurate in some cases.

For this reason, the fracture mechanics based model proposed by Zhang et al. [31] for NSM-strengthened concrete, is modified for NSM-strengthened masonry components in this section. In this model, the flexural tensile strength of masonry is substituted for the compressive strength in Eqs. (11) and (14) leading to the following expressions (knowing that  $\sqrt{f_c} = \frac{f_{ut}}{0.53}$ ):

$$G_f = 1.424\phi_f^{0.422}f_{ut}^{1.238} \quad (22)$$

$$\tau_{\max} = 4.09\phi_f^{0.138}f_{ut}^{1.226} \quad (23)$$

Substituting Eqs. (22-23) in Eqs. (10) and (12), the debonding force and the effective bond length in NSM-strengthened masonry can be obtained. Based on the available experimental database, the parameter  $\beta_L$ , in Eq. (15), is also modified. To this aim, the  $L_b/L_e$  is plotted against  $P/P_{\max}$  from the experimental results produced in this study. The best-fitted quadratic equation is then obtained as, see Fig 12:



$$\beta_L = \frac{L_b}{L_e} (2.36 - 1.36 \frac{L_b}{L_e}) \quad (24)$$

The accuracy of the model with the proposed modifications is presented in Fig 13 in comparison with the experimental results. The results obtained using the proposed model is compared with three existing models (specifically proposed for masonry structures) in Table 4. A good agreement with the experimental results is observed over a wide range of bond lengths. The model is able to predict an effective bond length in the specimens tested in the present study with high precision with an average of 188 mm (close to value estimated based on the experimental results). In addition, the predicted bond strength was improved in specimens with short bond lengths (30-150 mm), which are shown with red spots in Fig 13, having  $R^2$  of 0.8. A comparison between the proposed model with other available models for NSM-masonry systems, Table 5, shows this model produces reasonably accurate predictions with an average  $P/P_{\max}$  of 1.08 (CoV=23%).

## 7 Conclusions

An experimental investigation on the bond performance of Near Surface Mounted (NSM)-strengthened bricks was presented in this paper. The effect of test setup and anchorage method on the experimental results were initially investigated and discussed. The focus was then given to the effect of different parameters on the bond behavior including the bond length, groove size and loading conditions. The following conclusions can be drawn from the experimental results:

- 1) The test setup was found to have a significant influence on the failure mode and the debonding force of the specimens. This implies that comparisons with available data in the literature should be done with special care. A new test setup was developed in this study with the advantage, compared to conventional test setups, that no pre-compression load is applied on the specimens before testing.

- 2) The specimens with larger groove dimensions showed better bond performance in all bonded lengths without any change of failure mode. The presented results are however limited and a more extensive experimental study is still required for drawing conclusive remarks on the effect of groove size.
- 3) A significant increase of bond strength was observed in the specimens with increment of the bonded length from 30 mm to 120 mm bond length. The specimens with bonded lengths larger than 120 mm did not show significant change of debonding load implying that the effective bond length is in the range of 120-150 mm in the specimens tested in this study. Based on the experimental results, a new formula was proposed for modification of the bond strength in short bonded lengths.
- 4) The influence of cyclic loading on the global force-slip behavior was assessed. A slight in-cycle reduction of force and stiffness was observed in each displacement level after unloading-reloading. The results show the effect of cyclic loads on the bond performance can be significant and need to be considered at the design stage. The presented results are however limited and a comprehensive experimental program is necessary in future works for drawing clearer conclusions on the cyclic bond response and development of suitable constitutive laws.
- 5) Accuracy of the existing models in predicting the bond strength of a large number of experimental results was also evaluated. The results showed that most of the current strategies fail in accurate prediction of the effective bond length and consequently the bond strength. Based on the experimental results developed in this study, the formulation of the effective bond length was modified and a fracture-based bond strength model was proposed for NSM-strengthened masonry components.

## Acknowledgements

The second author acknowledges the financial support of the financial support of the European Union's Marie Curie Individual Fellowship program under REA grant agreement No. 701531.

## References

- [1] Seracino R, Jones NM, Ali MS, Page MW, Oehlers DJ. Bond strength of Near-Surface Mounted FRP strip-to-concrete joints. *J Compos Constr* 2007;11(4):401–9.
- [2] Petersen RB, Masia MJ, Seracino R. Bond behavior of Near-Surface Mounted FRP strips bonded to modern clay brick masonry prisms: Influence of strip orientation and compression perpendicular to the strip. *J Compos Constr* 2009;13(3):169–78.
- [3] De Lorenzis L, Tinazzi D, Nanni A. Near-Surface Mounted FRP rods for masonry strengthening : Bond and flexural testing. *Mecc. delle Strutt. Muratura Rinf. con FRP Mater.*, 2000.
- [4] Su Y, Wu C, Griffith MC. Modelling of the bond-slip behavior in FRP reinforced masonry. *Constr Build Mater* 2011;25(1):328–34.
- [5] Dizhur D, Griffith MC, Ingham JM. Pullout strength of NSM CFRP strips bonded to vintage clay brick masonry. *Eng Struct* 2014;69:25–36.
- [6] Dizhur D, Griffith M, Ingham J. Out-of-plane strengthening of unreinforced masonry walls using near surface mounted fibre reinforced polymer strips. *Eng Struct* 2014;59(2):330–43.
- [7] De Lorenzis L, Nanni A. Shear Strengthening of Reinforced Concrete Beams with Near-Surface Mounted Fiber-Reinforced Polymer Rods. *ACI Struct J* 2001;98(1):60–8.
- [8] Sharaky IA, Torres L, Baena M, Miàs C. An experimental study of different factors affecting the bond of NSM FRP bars in concrete. *Compos Struct* 2013;99:350–65.

- 1 [9] Khshain NT, Al-Mahaidi R, Abdouka K. Bond behaviour between NSM CFRP strips and  
2 concrete substrate using single-lap shear testing with epoxy adhesive. *Compos Struct*  
3 2015;132:205–14.
- 4 [10] Seracino R, Raizal Saifulnaz MR, Oehlers DJ. Generic Debonding Resistance of EB and  
5 NSM Plate-to-Concrete Joints. *J Compos Constr* 2007;11(1):62–70.
- 6 [11] Al-Saadi NTK, Mohammed A, Al-Mahaidi R. Performance of RC beams rehabilitated with  
7 NSM CFRP strips using innovative high-strength self-compacting cementitious adhesive  
8 (IHSSC-CA) made with graphene oxide. *Compos Struct* 2017;160:392–407.
- 9 [12] Seo SY, Feo L, Hui D. Bond strength of near surface-mounted FRP plate for retrofit of  
10 concrete structures. *Compos Struct* 2013;95:719–27.
- 11 [13] Capozucca R. Analysis of bond-slip effects in RC beams strengthened with NSM CFRP  
12 rods. *Compos Struct* 2013;102:110–23.
- 13 [14] Mohammed A, Tareq N, Al-saadi K, Al-mahaidi R. Assessment of bond strength of NSM  
14 CFRP strips embedded in concrete using cementitious adhesive made with graphene oxide.  
15 *Constr Build Mater* 2017;154:504–13.
- 16 [15] Zhang SS, Yu T. Effect of groove spacing on bond strength of Near-Surface Mounted (   
17 NSM ) bonded joints with multiple FRP strips 2017;155:103–13.
- 18 [16] Turco V, Galati N, De Lorenzis L, Modena C, Nanni A. Bond between Near Surface  
19 Mounted FRP rods and masonry in structural strengthening. *Adv. with Compos. plast, Ed.*  
20 *I, Crivelli-Visconti, Milan, Italy: 2003, p. 209–17.*
- 21 [17] Konthesingha KMC, Masia MJ, Petersen RB, Page AW. Bond behaviour of NSM FRP  
22 strips to modern clay brick. 11th Candian Mason. Symp., Toronto, Ontario: 2009.
- 23 [18] Kashyap J, Willis CR, Griffith MC, Ingham JM, Masia MJ. Debonding resistance of FRP-

- to-clay brick masonry joints. *Eng Struct* 2012;41:186–98.
- [19] De Lorenzis L, Nanni A. Characterization of FRP rods as Near-Surface Mounted Reinforcement. *J Compos Constr* 2001;5(2):114–21.
- [20] Coelho MRF, Sena-Cruz JM, Neves L a. C. A review on the bond behavior of FRP NSM systems in concrete. *Constr Build Mater* 2015;93:1157–69.
- [21] ASTM C67. Standard test methods for sampling and testing brick and structural clay tile. 2014.
- [22] EN 772-1. Methods of test for masonry units. Determination of compressive strength. BSI; 2011.
- [23] ASTM C39. Standard test method for compressive strength of cylindrical concrete specimens. 2016.
- [24] Fernandes PMG, Silva PM, Sena-Cruz J. Bond and flexural behavior of concrete elements strengthened with NSM CFRP laminate strips under fatigue loading. *Eng Struct* 2015;84:350–61.
- [25] Maljaee H, Ghiassi B, Lourenço PB, Oliveira DV. Moisture-induced degradation of interfacial bond in FRP-strengthened masonry. *Compos Part B Eng* 2016;87:47–58.
- [26] Maljaee H, Ghiassi B, Lourenço PB, Oliveira DV. FRP–brick masonry bond degradation under hygrothermal conditions. *Compos Struct* 2016;147:143–54.
- [27] Hassan TK, Rizkalla SH. Bond mechanism of Near-Surface-Mounted Fiber-Reinforced Polymer bars for flexural strengthening of concrete structures 2011;(101):1–7.
- [28] De Lorenzis L, Rizzo A, La Tegola A. A modified pull-out test for bond of Near-Surface Mounted FRP rods in concrete. *Compos Part B Eng* 2002;33(8):589–603.
- [29] Liu Y, Dawe J, McInerney J. Behaviour of GFRP sheets bonded to masonry walls. *Proc.*

1 Int. Symp. Bond Behav. FRP Struct., 2005, p. 473–80.

2 [30] Willis CR, Yang Q, Seracino R, Griffith MC. Bond behaviour of FRP-to-clay brick masonry  
3 joints. Eng Struct 2009;31(11):2580–7.

4 [31] Zhang SS, Teng JG, Yu T. Bond strength model for CFRP Strips Near-Surface Mounted to  
5 concrete. J Compos Constr 2014;18(3).

6 [32] Cruz JS, Barros J. Modeling of bond between Near-Surface Mounted CFRP laminate strips  
7 and concrete. Comput Struct 2004;82(17–19):1513–21.

8 [33] Zhang SS, Teng JG, Yu T. Bond–slip model for CFRP strips near-surface mounted to  
9 concrete. Eng Struct 2013;56:945–53.

10

11

## List of Tables

Table 1. Material properties.....	24
Table 2. Cyclic loading conditions. ....	25
Table 3. Database of experimental results on NSM-to-masonry bond behavior.....	26
Table 4. Comparison of analytical and experimental results.....	29
Table 5. $P_{exp}/P_{num}$ . ....	32

## List of Figures

Fig 1. Position of tapes inside the groove.	
Fig 2. Geometry of the test specimens and the test setup (dimensions are in mm).	
Fig 3. Test setup improvements.	
Fig 4. The load history of static cyclic tests.	
Fig 5. Typical failure modes.	
Fig 6. Load-displacement curves obtained from (a) ) Test setup 1; (b) ) Test setup 2; (c) Test setup 3.	
Fig 7. Effect of groove size on the debonding force.	
Fig 8. Variation of failure mode in each series with bond length.	
Fig 9. (a) Envelope of force-slip relationship and (b) variation of debonding force with bonded length.	
Fig 10. (a) Load-slip response under cyclic loading (b) in-cycle degradation trend.	
Fig 11. Evaluation of existing bond strength models: (a) Seracino et al. [10] (b) Zhang et al. [31] (c) Kashyap et al. [18] (Generic) (d) Kashyap et al. [18] (NSM) and (e) Willis et al. [31].	
Fig 12. The best fitted curve for the predicted effective bond length.	
Fig 13. Accuracy of proposed model.	

1 Table 1. Material properties.

	Compressive strength	Tensile strength	Elastic modulus
	(MPa)	(MPa)	(GPa)
Masonry brick	14.5	1.6	—
Epoxy adhesive	—	22.0	7.2
CFRP laminate	—	—	165.0

2



1 Table 2. Cyclic loading conditions.

Specimen	Number of cycles in each interval	First cycle (mm)	Displacement levels (mm)	Failure at cycle
1	3	4	4-5-6-7-8	14
2	3	4	4-5-6-7-7.5-8	16
3	3	5	5-6-7-8	10

2

1 Table 3. Database of experimental results on NSM-to-masonry bond behavior.

Reference	ID	Specimen	FRP		Groove size			$L_b$ (mm)	$f_{ut}$ (MPa)	$\phi_f$	$L_{per}$
			$t$ (mm)	$b$ (mm)	$E$ (GPa)	$d_g$ (mm)	$w_g$ (mm)				
	1	E-10-SS	6.35	6.3	40.8	7.35	8.35	254	1.93	0.88	23.05
	2	E-15-SS	6.35	6.3	40.8	7.35	8.35	381	1.93	0.88	23.05
	3	1A	2.80	15	207	16	4.80	355	3.57	3.33	36.80
	4	2A	2.80	15	207	16	4.80	355	3.57	3.33	36.80
	5	2B	2.80	15	207	16	4.80	355	3.57	3.33	36.80
	6	2C	2.80	15	207	16	4.80	355	3.57	3.33	36.80
	7	S1-A	2.80	15	207	16	4.80	336	3.57	3.33	36.80
	8	S1-B-NG	2.80	15	207	16	4.80	336	3.57	3.33	36.80
	9	S1-C-SG	2.80	15	207	16	4.80	336	3.57	3.33	36.80
	10	M-SG-3.6-10	3.60	10	165	11	5.60	420	3.41	1.96	27.60
	11	M-NSG-4.2-10	4.20	10	165	11	6.20	420	3.41	1.77	28.20
	12	M-NSG-7.2-10	7.20	10	165	11	9.20	420	3.41	1.20	31.20
	13	M-NSG-4.8-7.5	4.80	7.5	165	8.5	6.80	420	3.41	1.25	23.80
	14	M-NSG-4.8-5	4.80	5	165	6	6.80	420	3.41	0.88	18.80
	15	St1.0-3-10-1/2	1.20	10	162	11	3.20	244	3.55	3.44	25.20
	16	St1.0-3-15-1/2	1.20	15	162	16	3.20	241	3.55	5.00	35.20
	17	HO1.5-4-15-1/4	1.20	15	162	16	3.20	328	3.55	5.00	35.20
	18	HO1.5-4-15-1/4-N	1.20	15	162	16	3.20	334	3.55	5.00	35.20
	19	HO1.0-4-15-0	1.20	15	162	16	3.20	328	3.55	5.00	35.20
	20	HO1.0-4-15-0-N	1.20	15	162	16	3.20	334	3.55	5.00	35.20
	21	St1.0-4-15-1/2	1.20	15	162	16	3.20	328	3.55	5.00	35.20
	22	HO1.5-4-15-1/6	1.20	15	162	16	3.20	328	3.55	5.00	35.20
	23	HO1.5-4-15-1/4	1.20	15	162	16	3.20	328	3.55	5.00	35.20
	24	HO1.5-4-20-1/2	1.20	20	162	21	3.20	328	3.55	6.56	45.20
	25	St1.0-4-20-AC	1.20	20	162	20	3.20	328	3.55	6.25	43.20
	26	St1.0-4-20-BC	1.20	20	162	21	3.20	328	3.55	6.56	45.20
	27	A1-4-15-(6/20)	1.20	15	155	20	6.0	320	3.80	3.33	46.00
	28	A2-4-15-(6/20)	1.20	15	155	20	6.0	315	3.80	3.33	46.00
	29	A3-4-15-(6/20)	1.20	15	155	20	6.0	325	3.80	3.33	46.00
	30	A4-4-152-(6/20)	2.40	15	155	20	6.0	310	3.80	3.33	46.00
	31	A5-4-152-(6/20)	2.40	15	155	20	6.0	315	3.80	3.33	46.00
	32	B1-4-15-(6/20)	1.20	15	155	20	6.0	560	2.60	3.33	46.00
	33	B2-4-15-(7/20)	1.20	15	155	20	7.0	340	2.60	2.86	47.00
	34	B4-4-15-(3/20)	1.20	15	155	20	3.0	350	2.60	6.67	43.00
	35	B6-4-15-(12/20)	1.20	15	155	20	12.0	350	2.60	1.67	52.00
	36	B7-4-10-(6/15)	1.20	10	155	15	6.0	350	2.60	2.50	36.00
	37	B8-4-10-(6/15)	1.20	10	155	15	6.0	360	2.60	2.50	36.00
	38	B9-4-20-(7/25)	1.20	20	155	25	7.0	380	2.60	3.57	57.00

39	B10-4-25-(6/30)	1.20	25	155	30	6.0	360	2.60	5.00	66.00
40	B13-4-15-(6/30)	1.20	15	155	30	6.0	360	2.60	5.00	66.00
41	B14-4-15-(6/35)	1.20	15	155	35	6.0	450	2.60	5.83	76.00
42	B15-4-152-(7/20)	2.40	15	155	20	7.0	350	2.60	2.86	47.00
43	B16-5-15-(6/20)	1.20	15	155	20	6.0	360	2.60	3.33	46.00
44	B17-4-15-(6/25)	1.20	15	155	25	6.0	265	2.60	4.17	56.00
45	B18-4-30-(6/35)	1.20	30	155	35	6.0	260	2.60	5.83	76.00
46	B19-3-15-(6/20)	1.20	15	155	20	6.0	180	2.60	3.33	46.00
47	B20-3-30-(6/20)	1.20	10	155	20	6.0	180	2.60	3.33	46.00
48	B21-2-15-(6/20)	1.20	15	155	20	6.0	310	2.60	3.33	46.00
49	B22-1-20-(6/20)	1.20	20	155	20	6.0	310	2.60	3.33	46.00
50	C2-4-25-(6/30)	1.20	25	155	30	6.0	310	3.40	5.00	66.00
51	C5-4-15-(6/20)	1.20	15	155	20	6.0	310	3.40	3.33	46.00
52	C6-4-152-(6/20)	1.20	15	155	20	6.0	310	3.40	3.33	46.00
53	D2-4-15-(7/20)	1.20	15	155	20	7.0	350	2.50	2.86	47.00
54	E1-4-15-(6/20)	2.40	15	155	20	6.0	330	1.90	3.33	46.00
55	F1-4-15-(6/20)	1.20	15	155	20	6.0	330	1.20	3.33	46.00
56	F2-4-15-(6/20)	1.20	15	155	20	6.0	330	1.20	3.33	46.00
57	C2G3B30_1	1.40	10	165	13	3.0	30	1.60	4.33	29.00
58	C2G3B30_2	1.40	10	165	13	3.0	30	1.60	4.33	29.00
59	C2G3B30_3	1.40	10	165	13	3.0	30	1.60	4.33	29.00
60	C2G3B60_1	1.40	10	165	13	3.0	60	1.60	4.33	29.00
61	C2G3B60_2	1.40	10	165	13	3.0	60	1.60	4.33	29.00
62	C2G3B60_3	1.40	10	165	13	3.0	60	1.60	4.33	29.00
63	C2G3B90_1	1.40	10	165	13	3.0	90	1.60	4.33	29.00
64	C2G3B90_2	1.40	10	165	13	3.0	90	1.60	4.33	29.00
65	C2G3B90_3	1.40	10	165	13	3.0	90	1.60	4.33	29.00
66	C3G5B30_1	1.40	10	165	16	5.4	30	1.60	3.00	37.80
67	C3G5B30_2	1.40	10	165	16	5.4	30	1.60	3.00	37.80
68	C3G5B30_4	1.40	10	165	15	5.3	30	1.60	2.91	36.10
69	C3G5B30_5	1.40	10	165	16.3	5.4	30	1.60	3.02	38.00
70	C3G5B60_1	1.40	10	165	14.7	5.3	60	1.60	2.77	34.70
71	C3G5B60_2	1.40	10	165	15.7	5.3	60	1.60	2.96	36.70
72	C3G5B60_3	1.40	10	165	16.7	5.2	60	1.60	3.21	38.60
73	C3G5B60_4	1.40	10	165	15.3	5.3	60	1.60	2.89	35.90
74	C3G5B60_5	1.40	10	165	16.1	5.4	60	1.60	2.98	37.60
75	C3G5B90_1	1.40	10	165	15.5	5.3	90	1.60	2.92	36.30
76	C3G5B90_2	1.40	10	165	15.8	5.4	90	1.60	2.93	37.00
77	C3G5B90_3	1.40	10	165	15.2	5.2	90	1.60	2.92	35.60
78	C3G5B90_4	1.40	10	165	15.2	5.2	90	1.60	2.92	35.60
79	C3G5B90_5	1.40	10	165	16.4	5.3	90	1.60	3.09	38.10
80	C3G5B120_1	1.40	10	165	16.3	5.3	120	1.60	3.08	37.90
81	C3G5B120_2	1.40	10	165	15.5	5.4	120	1.60	2.87	36.40
82	C3G5B120_3	1.40	10	165	15.6	5.3	120	1.60	2.94	36.50
83	C3G5B120_4	1.40	10	165	15.5	5.3	120	1.60	2.92	36.30

84	C3G5B120_5	1.40	10	165	15.5	5.3	120	1.60	2.92	36.30
85	C3G5B150_1	1.40	10	165	15.7	5.6	150	1.60	2.80	37.00
86	C3G5B150_2	1.40	10	165	16.0	5.4	150	1.60	2.96	37.40
87	C3G5B150_4	1.40	10	165	16.2	5.3	150	1.60	3.06	37.70
89	C3G5B150_5	1.40	10	165	15.8	5.3	150	1.60	2.98	36.90

1

2

1 Table 4. Comparison of analytical and experimental results.

ID	Bond length	Effective bond length			Willis et al.		Kahsyap et al. (Generic)		Kahsyap et al. (NSM)		Proposed	
		Willis et al.	Kahsyap et al.	Proposed	$P_{num}$	$P_{exp}/P_{num}$	$P_{num}$	$P_{exp}/P_{num}$	$P_{num}$	$P_{exp}/P_{num}$	$P_{num}$	$P_{exp}/P_{num}$
1	254	212.0	112.56	155.9	12.81	1.50	16.29	1.1	22.40	0.86	11.93	1.61
2	381	212.0	112.56	155.9	12.81	1.45	16.29	1.1	22.40	0.83	11.93	1.55
3	355	310.3	255.02	215.2	76.39	0.81	81.37	0.7	74.05	0.83	67.17	0.92
4	355	310.3	255.02	215.2	76.39	0.85	81.37	0.8	74.05	0.88	67.17	0.97
5	355	310.3	255.02	215.2	76.39	0.83	81.37	0.7	74.05	0.86	67.17	0.95
6	355	310.3	255.02	215.2	76.39	0.87	81.37	0.8	74.05	0.90	67.17	0.99
7	336	310.3	255.02	215.2	76.39	1.03	81.37	0.9	74.05	1.06	67.17	1.17
8	336	310.3	255.02	215.2	76.39	0.85	81.37	0.8	74.05	0.88	67.17	0.97
9	336	310.3	255.02	215.2	76.39	0.95	81.37	0.8	74.05	0.98	67.17	1.08
10	420	294.5	235.37	203.2	46.29	1.40	51.56	1.2	55.27	1.18	41.80	1.55
11	420	311.3	250.49	215.5	49.20	1.14	55.21	1.0	61.09	0.92	44.67	1.26
12	420	366.9	306.92	260.7	61.08	1.10	70.55	0.9	88.21	0.76	56.60	1.19
13	420	299.1	248.93	211.7	38.17	1.56	43.94	1.3	54.19	1.10	35.29	1.68
14	420	259.0	225.52	189.6	25.27	1.77	29.84	1.5	41.00	1.09	23.79	1.88
15	244	178.0	145.68	123.7	30.03	0.92	31.94	0.8	28.79	0.96	26.36	1.05
16	241	182.7	153.25	131.7	47.97	0.98	49.65	0.9	39.84	1.17	41.30	1.13
17	328	182.7	153.25	131.7	47.97	0.92	49.65	0.8	39.84	1.10	41.30	1.07
18	334	182.7	153.25	131.7	47.97	1.06	49.65	1.0	39.84	1.27	41.30	1.23
19	328	182.7	153.25	131.7	47.97	0.80	49.65	0.7	39.84	0.96	41.30	0.93
20	334	182.7	153.25	131.7	47.97	0.97	49.65	0.9	39.84	1.17	41.30	1.13
21	328	182.7	153.25	131.7	47.97	0.87	49.65	0.8	39.84	1.04	41.30	1.00
22	328	182.7	153.25	131.7	47.97	0.87	49.65	0.8	39.84	1.05	41.30	1.01
23	328	182.7	153.25	131.7	47.97	0.80	49.65	0.7	39.84	0.96	41.30	0.93
24	328	181.5	157.86	136.9	67.43	0.73	68.41	0.7	50.46	0.98	57.23	0.86
25	328	186.7	161.16	139.5	65.08	0.77	66.26	0.7	49.62	1.01	55.38	0.90
26	328	181.5	157.86	136.9	67.43	0.76	68.41	0.7	50.46	1.01	57.23	0.89
27	320	151.4	131.41	105.0	50.23	0.74	53.07	0.7	48.29	0.77	44.22	0.84
28	315	151.4	131.41	105.0	50.23	0.99	53.07	0.9	48.29	1.03	44.22	1.12
29	325	151.4	131.41	105.0	50.23	1.01	53.07	0.9	48.29	1.05	44.22	1.14
30	310	214.2	185.84	148.5	71.03	0.85	75.06	0.8	68.30	0.89	62.54	0.97
31	315	214.2	185.84	148.5	71.03	0.92	75.06	0.8	68.30	0.95	62.54	1.04
32	560	190.2	118.61	132.2	40.00	1.18	44.40	1.0	40.40	1.17	34.96	1.35
33	340	187.2	116.62	129.3	38.83	1.03	43.59	0.9	41.60	0.96	34.21	1.17
34	350	189.6	126.13	143.8	46.41	0.76	48.97	0.7	35.95	0.98	39.13	0.90
35	350	169.8	108.51	118.2	35.44	1.01	41.39	0.8	46.68	0.76	32.11	1.11
36	350	173.3	108.22	119.5	26.79	0.87	30.37	0.7	30.21	0.77	23.77	0.98

37	360	173.3	108.22	119.5	26.79	0.99	30.37	0.8	30.21	0.88	23.77	1.12
38	380	197.4	123.38	137.8	52.36	0.80	57.83	0.7	51.51	0.81	45.60	0.92
39	360	203.2	129.93	146.7	68.81	0.72	74.16	0.6	59.51	0.84	58.89	0.85
40	360	157.4	100.64	113.7	53.30	0.62	57.45	0.5	46.10	0.71	45.62	0.72
41	450	144.8	94.37	107.1	59.57	0.60	63.48	0.5	48.56	0.73	50.57	0.70
42	350	264.8	164.93	182.9	54.91	0.97	61.64	0.8	58.84	0.91	48.38	1.10
43	360	190.2	118.61	132.2	40.00	0.86	44.40	0.7	40.40	0.85	34.96	0.99
44	265	172.2	108.46	121.8	46.80	0.53	51.11	0.4	43.40	0.57	40.44	0.62
45	260	204.8	133.46	151.5	84.24	0.53	89.77	0.5	68.68	0.65	71.52	0.63
46	180	190.2	118.61	132.2	37.85	1.02	44.40	0.8	40.40	0.96	34.96	1.10
47	80	155.3	96.85	107.9	16.82	1.50	29.95	0.8	27.25	0.92	28.60	0.88
48	310	190.2	118.61	132.2	40.00	0.87	44.40	0.7	40.40	0.86	34.96	1.00
49	310	219.6	136.96	152.6	46.19	0.39	51.27	0.3	46.65	0.38	40.37	0.44
50	310	172.9	139.69	124.7	80.83	0.75	84.13	0.7	67.51	0.89	69.53	0.87
51	310	161.9	127.52	112.3	46.98	0.92	50.37	0.8	45.83	0.94	41.28	1.05
52	310	161.9	127.52	112.3	46.98	1.03	50.37	0.9	45.83	1.06	41.28	1.17
53	350	191.7	115.39	132.4	37.92	0.90	42.79	0.8	40.84	0.83	33.39	1.02
54	330	324.7	154.12	226.2	46.86	0.61	54.19	0.5	49.31	0.58	40.72	0.70
55	330	302.4	96.26	211.4	25.15	0.83	30.87	0.6	28.09	0.74	21.66	0.96
56	330	302.4	96.26	211.4	25.15	0.78	30.87	0.6	28.09	0.70	21.66	0.91
57	30	291.1	120.49	207.3	2.38	4.32	6.68	1.5	5.61	1.84	6.19	1.67
58	30	291.1	120.49	207.3	2.38	4.65	6.68	1.6	5.61	1.98	6.19	1.79
59	30	291.1	120.49	207.3	2.38	4.88	6.68	1.7	5.61	2.08	6.19	1.88
60	60	291.1	120.49	207.3	4.77	2.56	13.37	0.9	11.21	1.09	11.25	1.09
61	60	291.1	120.49	207.3	4.77	3.36	13.37	1.2	11.21	1.43	11.25	1.42
62	60	291.1	120.49	207.3	4.77	2.90	13.37	1.0	11.21	1.23	11.25	1.23
63	90	291.1	120.49	207.3	7.15	1.96	20.05	0.7	16.82	0.83	15.18	0.92
64	90	291.1	120.49	207.3	7.15	2.14	20.05	0.7	16.82	0.91	15.18	1.01
65	90	291.1	120.49	207.3	7.15	2.41	20.05	0.8	16.82	1.02	15.18	1.13
66	30	254.7	103.99	176.8	2.82	3.08	8.24	1.0	7.75	1.12	7.54	1.15
67	30	254.7	103.99	176.8	2.82	3.54	8.24	1.2	7.75	1.29	7.54	1.33
68	30	260.3	106.28	180.5	2.68	3.18	7.84	1.0	7.44	1.15	7.19	1.19
69	30	254.1	103.74	176.4	2.84	3.78	8.29	1.3	7.78	1.38	7.59	1.42
70	60	264.9	108.20	183.5	5.10	2.85	14.96	0.9	14.41	1.01	12.32	1.18
71	60	258.4	105.49	179.3	5.47	2.62	15.98	0.9	15.08	0.95	13.08	1.09
72	60	252.6	103.19	175.8	5.86	2.57	17.01	0.8	15.66	0.96	13.85	1.09
73	60	261.0	106.55	180.9	5.32	2.86	15.57	0.9	14.81	1.03	12.78	1.19
74	60	255.3	104.24	177.2	5.61	2.13	16.38	0.7	15.43	0.77	13.38	0.89
75	90	259.7	106.01	180.1	8.09	2.32	23.66	0.7	22.42	0.84	17.09	1.10
76	90	257.2	105.01	178.4	8.25	2.04	24.12	0.7	22.85	0.74	17.35	0.97
77	90	262.2	107.05	181.8	7.93	2.47	23.20	0.8	21.99	0.89	16.83	1.16
78	90	262.2	107.05	181.8	7.93	2.26	23.20	0.7	21.99	0.81	16.83	1.06
79	90	254.0	103.71	176.5	8.60	1.82	25.04	0.6	23.32	0.67	17.93	0.87
80	120	254.6	103.96	176.9	11.39	1.68	28.75	0.6	26.82	0.71	20.50	0.93
81	120	259.1	105.79	179.6	10.77	1.90	27.81	0.7	26.50	0.77	19.69	1.04

82	120	259.0	105.75	179.7	10.86	1.97	27.98	0.7	26.46	0.81	19.81	1.08
83	120	259.7	106.01	180.1	10.79	1.99	27.87	0.7	26.41	0.81	19.72	1.09
84	120	259.7	106.01	180.1	10.79	1.69	27.87	0.6	26.41	0.69	19.72	0.93
85	150	256.7	104.83	177.8	13.62	1.57	27.91	0.7	26.80	0.80	20.84	1.03
86	150	255.9	104.50	177.6	13.93	1.54	28.36	0.7	26.76	0.80	21.20	1.01
87	150	255.2	104.21	177.3	14.14	1.45	28.64	0.7	26.77	0.76	21.42	0.96
89	150	257.7	105.23	178.9	13.76	1.40	28.20	0.6	26.56	0.73	21.07	0.92

1

1 Table 5.  $P_{\text{exp}}/P_{\text{num}}$ .

model	mean	max	min	CoV (%)
Proposed	1.08	1.88	0.44	23
Willis et al. [30]	1.52	4.88	0.39	64
Kashyap et al. (Generic) [18]	0.87	1.74	0.35	28
Kashyap et al. (NSM) [18]	0.95	2.08	0.38	27
Seracino et al. [10]	0.51	1.44	0.14	54
Zhange et al. [31]	0.31	0.52	0.14	24

2





Fig 1. Position of tapes inside the groove.

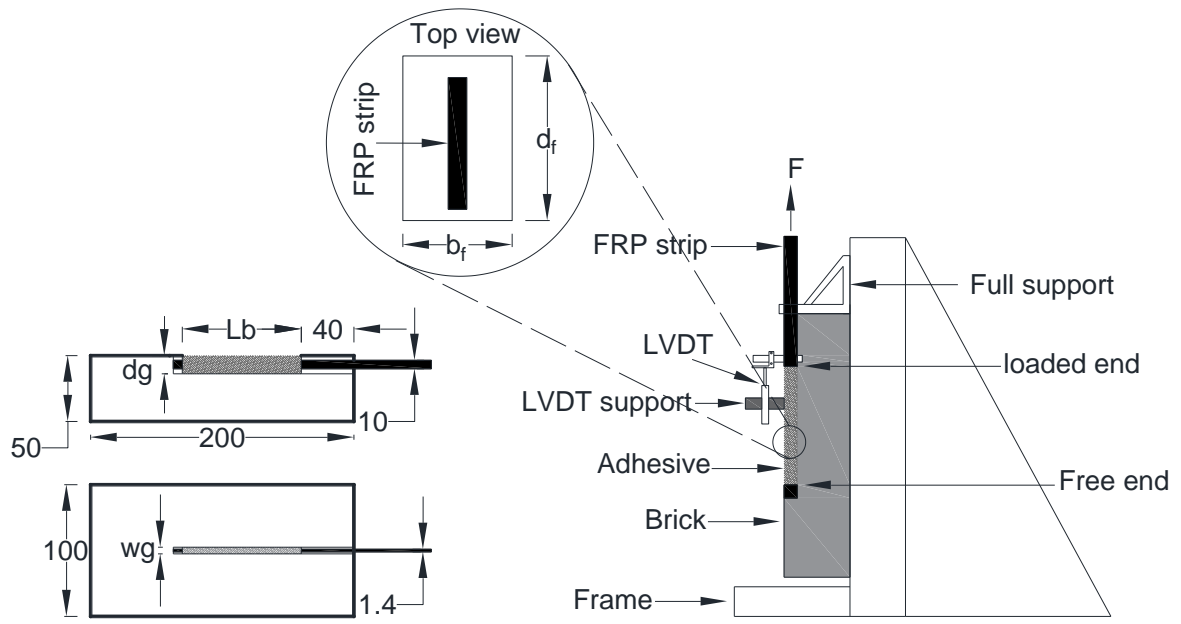
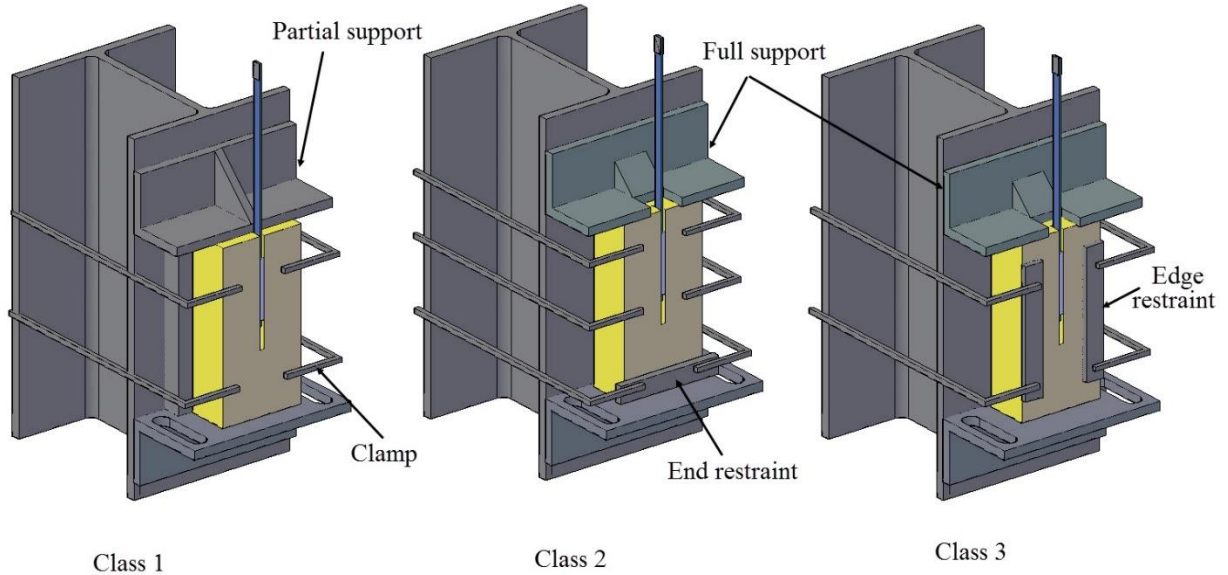


Fig 2. Geometry of the test specimens and the test setup (dimensions are in mm).

1



2

3

4

Fig 3. Test setup improvements.

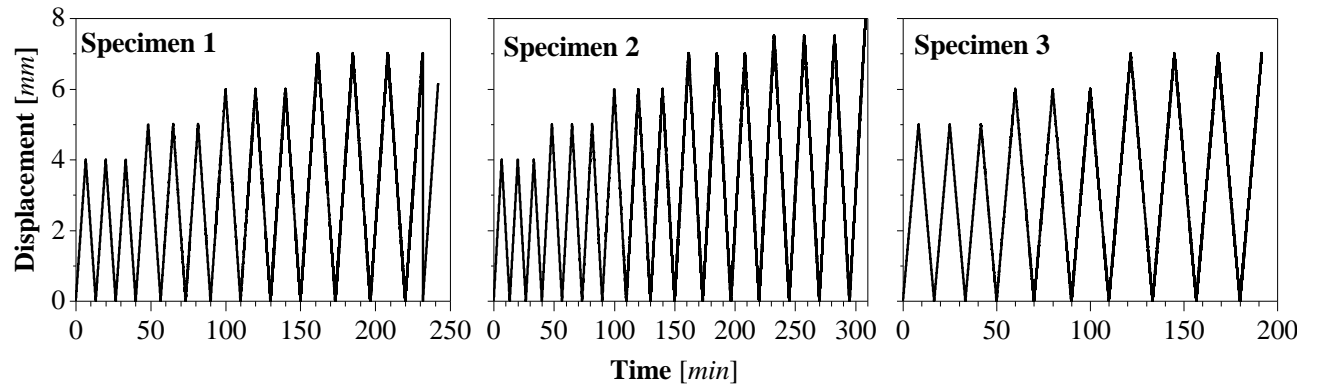


Fig 4. The load history of static cyclic tests.

A (Splitting)



B (Full debonding with diagonal cracks)



C (Interface)

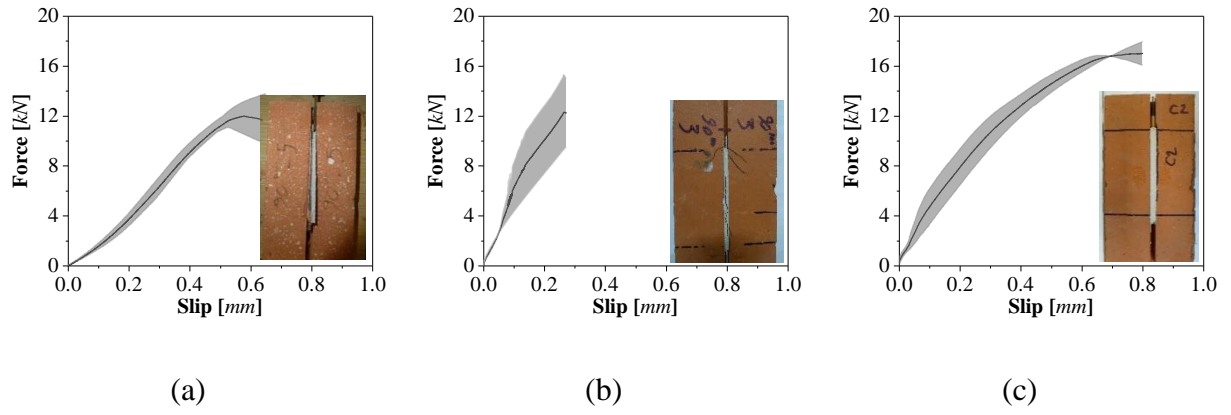


Fig 5. Typical failure modes.

1

2

1



2 Fig 6. Load-displacement curves obtained from (a) Test setup 1; (b) Test setup 2; (c) Test setup

3 3.

4

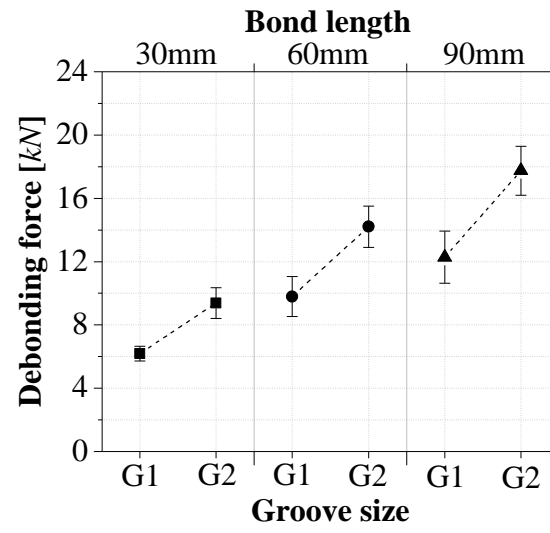
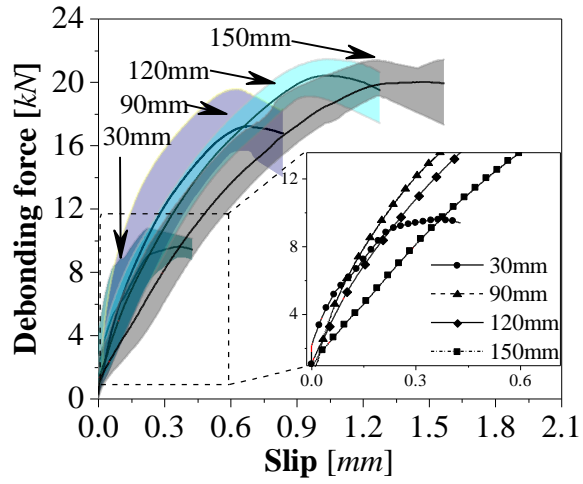
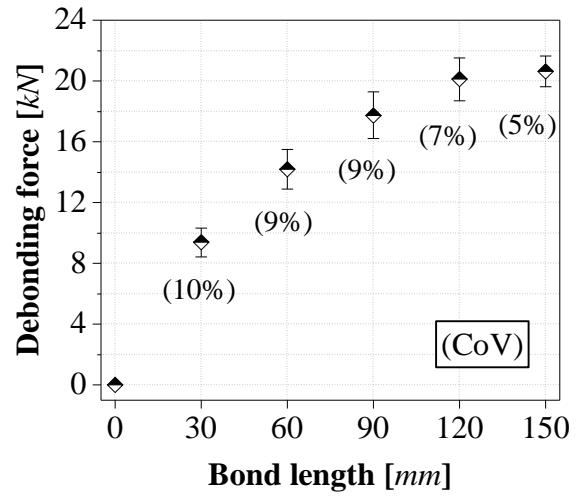


Fig 7. Effect of groove size on the debonding force.



(a)



(b)

Fig 8. (a) Envelope of force-slip relationship and (b) variation of debonding force with bonded length.



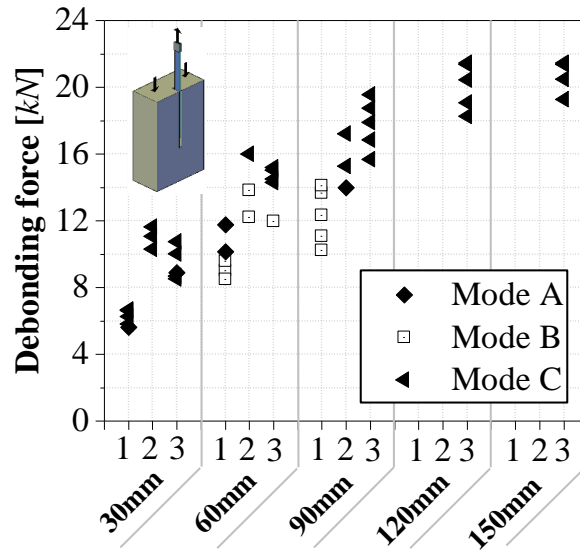
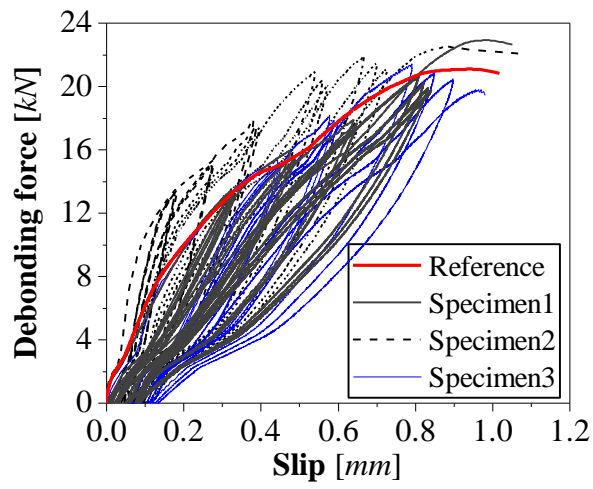
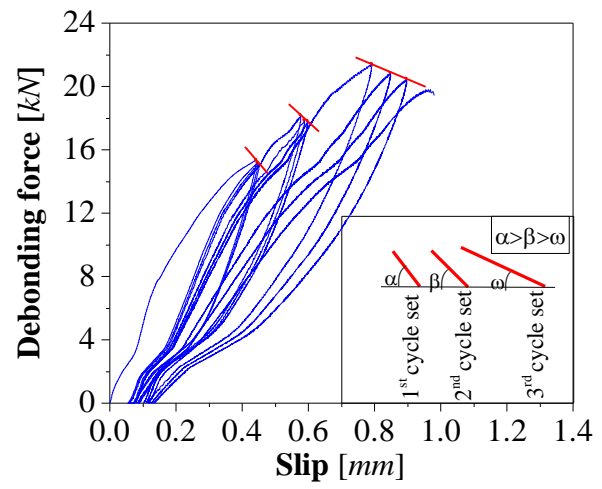


Fig 9. Variation of failure mode in each series with bond length.

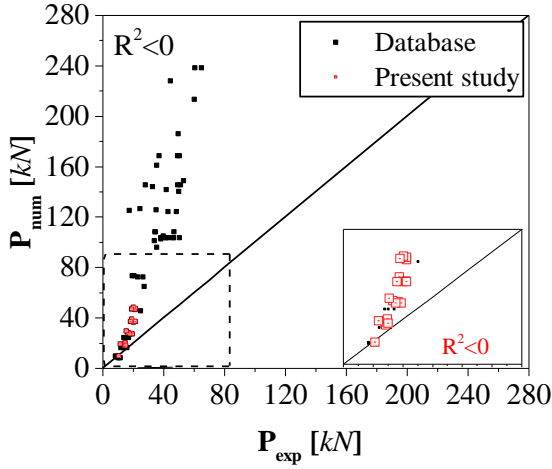


(a)

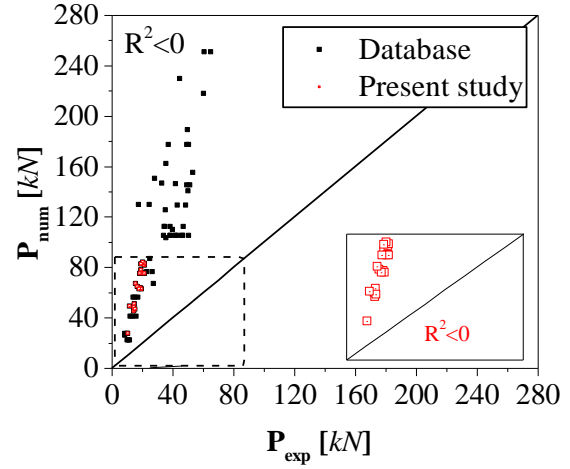


(b)

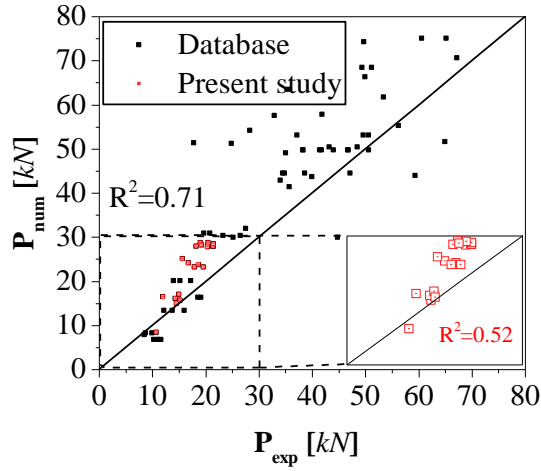
Fig 10. (a) Load-slip response under cyclic loading (b) in-cycle degradation trend.



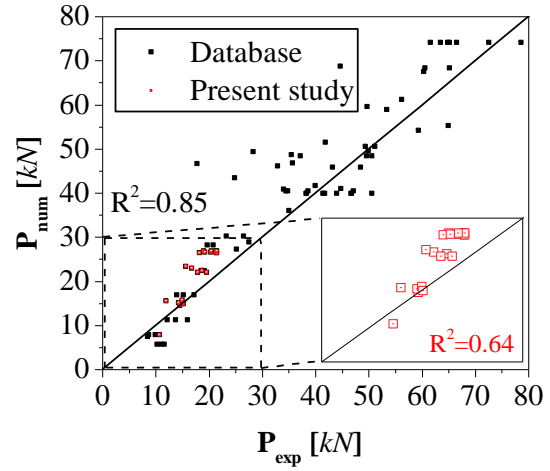
(a)



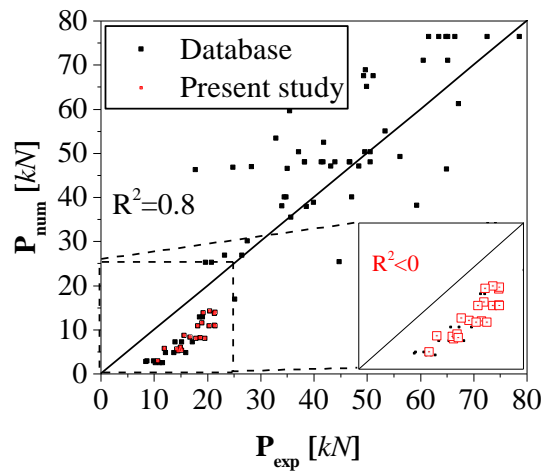
(b)



(c)



(d)



(e)

1 Fig 11. Evaluation of existing bond strength models: (a) Seracino et al. [10] (b) Zhang et al. [31]  
2 (c) Kashyap et al. [18] (Generic) (d) Kashyap et al. [18] (NSM) and (e) Willis et al. [31].

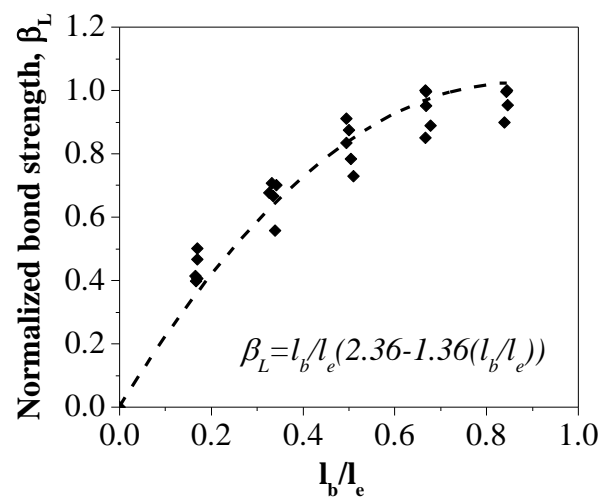


Fig 12. The best fitted curve for the predicted effective bond length.

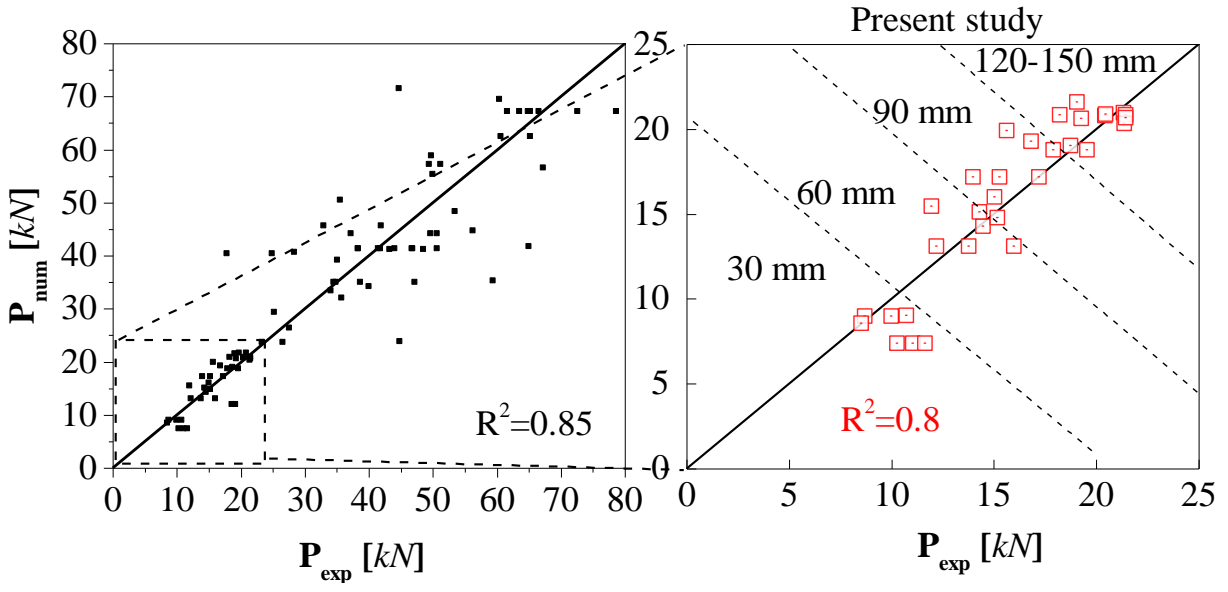


Fig 13. Accuracy of proposed model.